

AD-A242 443



## REPORT DOCUMENTATION PAGE

STE

8 1991

C

D

25 DECLASSIFICATION/DOWNGRADING SCHEDULE

15 RESTRICTIVE MARKINGS

3 DISTRIBUTION AVAILABILITY OF REPORT

Unclassified/Unlimited

4 PERFORMING ORGANIZATION REPORT NUMBER(S)

5. MONITORING ORGANIZATION REPORT NUMBER(S)

ONR Technical Report 1

6a. NAME OF PERFORMING ORGANIZATION  
Dept of Chemical Engineering  
and Materials Science6b. OFFICE SYMBOL  
(If applicable)  
Code 11137a. NAME OF MONITORING ORGANIZATION  
Office of Naval Research

6c. ADDRESS (City, State, and ZIP Code)

University of Minnesota  
Minneapolis, MN 55455

7b. ADDRESS (City, State, and ZIP Code)

800 North Quincy Street  
Arlington, VA 222178a. NAME OF FUNDING/SPONSORING  
ORGANIZATION  
Office of Naval Research8b. OFFICE SYMBOL  
(If applicable)9. PROCUREMENT INSTRUMENT IDENTIFICATION NUMBER  
Contract No. N00014 91-J-1927

8c. ADDRESS (City, State, and ZIP Code)

800 North Quincy Street  
Arlington, VA 22217-5000

10 SOURCE OF FUNDING NUMBERS

PROGRAM  
ELEMENT NO.PROJECT  
NO.TASK  
NO.WORK UNIT  
ACCESSION NO.

11. TITLE (Include Security Classification)

Molecular and Electronic Structure of Thin Films of Protoporphyrin(IX)Fe(III)Cl

12. PERSONAL AUTHOR(S)

Shelly R. Snyder and Henry S. White

13a. TYPE OF REPORT  
Technical13b. TIME COVERED  
FROM 1/1/91 TO 10/31/9314. DATE OF REPORT (Year, Month, Day)  
November 10, 199115. PAGE COUNT  
44 pages

16. SUPPLEMENTARY NOTATION

prepared for publication in the Journal of American Chemical Society

17. COSATI CODES

FIELD GROUP SUB-GROUP

18. SUBJECT TERMS (Continue on reverse if necessary and identify by block number)

STM, Protoporphyrin, Electrochemistry

19 ABSTRACT (Continue on reverse if necessary and identify by block number)

Electrochemical, scanning tunneling microscopy (STM), and tunneling spectroscopy studies of the molecular and electronic properties of thin films of protoporphyrin(IX)Fe(III)Cl (abbreviated as PP(IX)Fe(III)Cl) on highly oriented pyrolytic graphite (HOPG) electrodes are reported. PP(IX)Fe(III)Cl films are prepared by two different methods: (1) adsorption, yielding an electrochemically-active film, and (2) irreversible electrooxidative polymerization, yielding an electrochemically-inactive film. STM images, in conjunction with electrochemical results, indicate that adsorption of PP(IX)Fe(III)Cl from aqueous solutions onto freshly cleaved HOPG results in a film comprised of molecular aggregates. In contrast, films prepared by irreversible electrooxidative polymerization of PP(IX)Fe(III)Cl have a denser, highly structured morphology, including what appear to be small pinholes (~50Å diameter) in an otherwise continuous film. Tunneling spectroscopy of adsorbed PP(IX)Fe(III)Cl on HOPG shows that the distribution of electronic states associated with the adsorbed electroactive film is described by two-quasi-gaussian peaks centered at  $\pm 0.5$  eV of the Fermi level.

(continued)

20 DISTRIBUTION AVAILABILITY OF ABSTRACT

☒ UNCLASSIFIED/UNLIMITED ☐ SAME AS RPT ☐ DTIC USERS

21 ABSTRACT SECURITY CLASSIFICATION

Unclassified

22a. NAME OF RESPONSIBLE INDIVIDUAL  
Henry S. White22b. TELEPHONE (Include Area Code) 22c. OFFICE SYMBOL  
(612) 625-6345

91 1115 002

19. Abstract continued

This density of state distribution is approximated closely by the Marcus-Gerisher model, suggesting a parallel mechanism of electron transfer in STM imaging and electrochemistry. The first-order rate constant for electron transfer between the STM tip and surface-confined PP(IX)Fe(III)Cl is estimated from an analysis of the tunneling current density to be  $\sim 10^{10} \text{s}^{-1}$ .

**91-15686**



OFFICE OF NAVAL RESEARCH

Contract N00014-91-J-1927

R&T Code 413v001

Technical Report No. 1

Accession For	
NTIS GRA&I	<input checked="" type="checkbox"/>
DTIC TAB	<input type="checkbox"/>
Unannounced	<input type="checkbox"/>
Justification	
By	
Distribution/	
Availability Codes	
Dist	Avail and/or Special
A-1	

MOLECULAR AND ELECTRONIC STRUCTURE OF THIN FILMS OF  
PROTOPORPHYRIN(IX)Fe(III)Cl

by

SHELLY R. SNYDER AND HENRY S. WHITE

Prepared for Publication in the  
JOURNAL OF THE AMERICAN CHEMICAL SOCIETY

University of Minnesota  
Department of Chemical Engineering and Materials Science  
Minneapolis, MN 55455

November 10, 1991

Reproduction in whole or in part is permitted for any purpose of the United States  
Government.

This document has been approved for public release and sale; its distribution is unlimited.

# MOLECULAR AND ELECTRONIC STRUCTURE OF THIN FILMS OF PROTOPORPHYRIN(IX)Fe(III)Cl

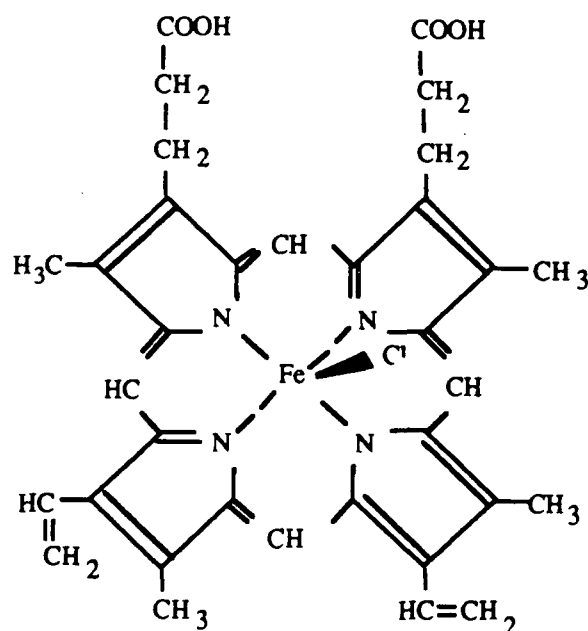
Shelly R. Snyder and Henry S. White  
Department of Chemical Engineering and Materials Science  
University of Minnesota  
Minneapolis, MN 55455

**ABSTRACT.** Electrochemical, scanning tunneling microscopy (STM), and tunneling spectroscopy studies of the molecular and electronic properties of thin films of protoporphyrin(IX)Fe(III)Cl (abbreviated as PP(IX)Fe(III)Cl) on highly oriented pyrolytic graphite (HOPG) electrodes are reported. PP(IX)Fe(III)Cl films are prepared by two different methods: (1) *adsorption*, yielding an electrochemically-active film, and (2) *irreversible electrooxidative polymerization*, yielding an electrochemically-inactive film. STM images, in conjunction with electrochemical results, indicate that adsorption of PP(IX)Fe(III)Cl from aqueous solutions onto freshly cleaved HOPG results in a film comprised of molecular aggregates. In contrast, films prepared by irreversible electrooxidative polymerization of PP(IX)Fe(III)Cl have a denser, highly structured morphology, including what appear to be small pinholes ( $\sim 50\text{\AA}$  diameter) in an otherwise continuous film. Tunneling spectroscopy of adsorbed PP(IX)Fe(III)Cl on HOPG shows that the distribution of electronic states associated with the adsorbed electroactive film is described by two quasi-gaussian peaks centered at  $\pm 0.5$  eV of the Fermi level. This density of state distribution is approximated closely by the Marcus-Gerisher model, suggesting a parallel mechanism of electron-transfer in STM imaging and electrochemistry. The first-order rate constant for electron transfer between the STM tip and surface-confined PP(IX)Fe(III)Cl is estimated from an analysis of the tunneling current density to be  $\sim 10^{10}\text{s}^{-1}$ .

Submitted to *J. Am. Chem. Soc.*, October, 1991.

## INTRODUCTION.

This paper presents an analysis of the structure and electronic properties of thin molecular films derived from protoporphyrin(IX)Fe(III)Cl (abbreviated hereafter as PP(IX)Fe(III)Cl). The redox chemistry of PP(IX)Fe(III)Cl and other metal porphyrins plays a key role in the biological activity of chlorophylls and cytochromes<sup>[1,2]</sup>, and has been investigated extensively in studies concerned with the elucidation of biological functions of protein molecules. The reversible binding of oxygen by various metalloporphyrins, including PP(IX)Fe(III)Cl, is a process similar to that which allows hemoglobin to transport oxygen<sup>[3]</sup> in biological tissues, and is also of interest as a model for the electrocatalytic reduction of O<sub>2</sub><sup>[4]</sup>.



The kinetics and electron-transfer mechanisms of the reduction of PP(IX)Fe(III)Cl and synthetic analogs have been studied in detail in aqueous and nonaqueous solvents <sup>[5]</sup>. Particularly relevant to the present investigation is the well known observation that PP(IX)Fe(III)Cl irreversibly adsorbs from aqueous solutions onto the surfaces of vitreous carbon and pyrolytic graphite electrodes <sup>[4b,6,7]</sup> and to a lesser extent onto the surface of

some metals (e.g., Hg)<sup>[4c,8]</sup>. Adsorption yields a molecularly-thin film that can be electroreduced at potentials near the pH-dependent thermodynamic solution value of PP(IX)Fe(III)Cl. The film also undergoes ligand substitution reactions in the presence of carbon monoxide and strong axial heterocyclic ligands (e.g., pyridine)<sup>[9]</sup> that are analogous to the known solution chemistry of PP(IX)Fe(III)Cl. Although small differences exist in the literature values, it is generally observed from coulometric analysis that approximately one monolayer of PP(IX)Fe(III)Cl is adsorbed onto the electrode surface, corresponding to a surface coverage of  $\sim 10^{-10}$  mole/cm<sup>2</sup>.

The molecular and intramolecular structure of adsorbed PP(IX)Fe(III)Cl layers is considerably less well understood than the corresponding electrochemical behavior. Surface coverage measurements of PP(IX)Fe(III)Cl, in conjunction with molecular models, have been used by several authors to imply that PP(IX)Fe(III)Cl adsorbs in a flat configuration with the aromatic system parallel to the electrode surface. To our knowledge, this simple and plausible structure has not been demonstrated by a direct imaging technique or by a spectroscopic method sensitive to the adsorbate orientation. Evidence also exists for more elaborate structures in which PP(IX)Fe(III)Cl is adsorbed as molecular aggregates or with multiple orientations with respect to the electrode surface. Brown et al.<sup>[7]</sup>, for example, observed two closely separated voltammetric reduction waves for PP(IX)Fe(III)Cl adsorbed on vitreous carbon in 0.1 M sodium borate solutions. These authors attributed the multiple waves to the presence of two distinct forms (albeit unknown) of PP(IX)Fe(III)Cl, presumably a result of specific differences in the orientation or interactions of the molecules on the surface. Electrochemical analyses showed that only one form of the adsorbed molecule is capable of reversible binding and reducing O<sub>2</sub> dissolved in solution, demonstrating an interesting difference between surface-confined and solution chemistry.

In this communication, we report the results of our investigation of the structure and electronic properties of PP(IX)Fe(III)Cl using scanning tunneling microscopy (STM) [10,11]. We show that electroactive films of PP(IX)Fe(III)Cl adsorbed on graphite from aqueous borate solutions are comprised mainly of large, uniformly distributed molecular aggregates. The structure of adsorbed PP(IX)Fe(III)Cl is also compared to electroinactive films prepared by electrooxidative polymerization of PP(IX)Fe(III)Cl. We also report an intriguing correlation of tunneling spectroscopy data with the electrochemical properties of adsorbed and polymerized films of PP(IX)Fe(III)Cl. In particular, we show that the surface distribution of electronic states (SDOS) obtained from TS experiments on thin electroactive films of adsorbed PP(IX)Fe(III)Cl is in good agreement with predictions from the classical electron-transfer theories of Marcus<sup>[12]</sup>, Gerischer<sup>[13]</sup>, Levich<sup>[14]</sup> and others<sup>[15]</sup>. Analysis of the tunneling current yields an apparent first-order electron-transfer rate constant of  $10^{10} \text{ s}^{-1}$  in the STM experiment. In contrast, the SDOS of thin films prepared by the irreversible, oxidative electropolymerization of PP(IX)Fe(III)Cl show a wide energy region that contains a low density of electronic states, in agreement with the reduced electrochemical activity.

## EXPERIMENTAL.

*Reagents.* Protoporphyrin(IX)Fe(III)Cl (Fluka) and analytical grade sodium borate ( $\text{Na}_2\text{B}_4\text{O}_7$ , Mallinckrodt) were used as received. Water was purified ( $18\text{M}\Omega$ ) with a Water Prodigy apparatus (Labconco Corp.).

*Instrumentation and Methods.* STM images were obtained in air with a Nanoscope II (Digital Instruments, Santa Barbara, CA.). Images were recorded in constant current mode using scan rates ranging from 2.5 to 5.6 Hz. Tunneling tips were constructed from mechanically cut Pt-70%-Rh 30% wire. Bias voltages and tunneling currents varied for

each image and are listed in the figure captions. Images are low-pass filtered. Current versus voltage, I-V, data were acquired at a constant tip-to-substrate separation. I-V plots were recorded by measuring the current between the tip and substrate while linearly scanning the voltage (with the tip-to-substrate separation bias voltage interrupted) between  $\pm 1.5$  V over a 0.2 sec. interval for the adsorbed PP(IX)Fe(III)Cl films and between  $\pm 2.0$  V over a 0.2 sec. interval for the electrooxidized PP(IX)Fe(III)Cl films. Tunneling currents observed in the I-V measurements ranged from 1 to 50 nA. Each I-V plot is comprised of  $\sim 10^{10}$  electron-transfer events (plus or minus one order of magnitude). Plots of  $(dI/dV)/(I/V)$  vs V (i.e., density of state plots (DOS)) were numerically calculated from the I-V curves following transfer of the data to an IBM PC.

Electrodes were prepared using a  $\sim 0.6 \times 0.6 \times 0.1$  cm piece of highly oriented pyrolytic graphite, HOPG, (Grade A or Grade B, Union Carbide). Electrical contact to the back side of the HOPG sample was made with a copper wire and conductive epoxy (Epo-tek H20E, Epoxy Technology Inc.). The HOPG substrate was mounted perpendicular to the end of a glass tube with epoxy, exposing both the front basal plane and edges to the solution. Following adsorption or electropolymerization of PP(IX)Fe(III)Cl, electrodes were rinsed with water and air dried. The HOPG substrate was removed intact from the glass tube for STM measurements by inserting a razor blade between the substrate and the epoxy.

Electrochemical experiments were performed with a EG&G Princeton Applied Research Model 173 Potentiostat and a Model 175 Universal Programmer. The electrochemical cell consisted of a sodium saturated calomel reference electrode (SCE), a platinum wire coil counter electrode, and the HOPG working electrode. Dissolved oxygen was removed from the solution by purging with prepurified  $N_2$  prior to experimentation (20 min.) and by maintaining a positive pressure of  $N_2$  in the cell above the solution during voltammetric measurements.

## RESULTS AND DISCUSSION.

**STM Images of PP(IX)Fe(III)Cl on HOPG.** The adsorption and subsequent electrochemical behavior of PP(IX)Fe(III)Cl on HOPG and glassy carbon electrodes has been investigated extensively in several laboratories<sup>[4b,6,7]</sup>. In addition, the electrochemical oxidation of the dimethylester analogue of PP(IX)Fe(III)Cl on Pt electrodes <sup>[16,17]</sup> has been studied by Macor and Spiro . However, to our knowledge no direct measurements of the surface structure of either electrode have been performed. Studies on porphyrin complexes have been hampered, in part, by the propensity of these complexes to aggregate under various solution conditions. In aqueous solutions, PP(IX)Fe(III)Cl is known to form aggregates<sup>[18,19]</sup> as large as ~4,000,000 MW <sup>[20]</sup>, although typical values are in the range of ~30,000 MW <sup>[21]</sup>. The aggregates are thought to involve both  $\mu$ -oxo bridged dimers <sup>[18,22]</sup> as well as larger oligomers where the complexes are associated through the vinyl groups <sup>[23]</sup>, and/or hydrogen bonded <sup>[24]</sup>.

Below we report the STM images of films of PP(IX)Fe(III)Cl on HOPG electrodes. We show that the structure and electronic properties of the resulting films vary significantly depending on whether PP(IX)Fe(III)Cl is deposited by adsorption or by electrooxidative polymerization.

### *Films formed by Adsorption:*

Molecular films of PP(IX)Fe(III)Cl were formed by adsorption onto HOPG following the procedure of Anson and coworkers <sup>[7]</sup>. A freshly cleaved HOPG electrode was placed in a 0.1 M Na<sub>2</sub>B<sub>4</sub>O<sub>7</sub> solution (pH ~10.0) containing ~0.5 mM PP(IX)Fe(III)Cl and the potential was cycled between 0.0 and -1.2 V vs SCE. This potential range encompasses the half-wave potential for the one-electron metal localized reduction of PP(IX)Fe(III)Cl ( $E_{1/2}$  ~ -0.52 V vs SCE). A diffusion-limited, peaked,

cyclic voltammogram corresponding to PP(IX)Fe(III)Cl reduction was observed in the deposition solution.

Fig. 1 shows the cyclic voltammetric response of an HOPG electrode in an aqueous solution containing only  $\text{Na}_2\text{B}_4\text{O}_7$  following adsorption of PP(IX)Fe(III)Cl. The voltammogram shows nearly symmetrical reduction and reoxidation waves of equal magnitude, consistent with reversible electron-transfer between the surface-bound redox species and HOPG. The surface coverage of PP(IX)Fe(III)Cl,  $\Gamma$ , estimated from the area under the voltammogram, is  $\sim 10 \times 10^{-10}$  moles/cm<sup>2</sup>. This value is uncorrected for adsorption of PP(IX)Fe(III)Cl on the exposed edged planes of the HOPG electrode and thus overestimates the true surface coverage of adsorbed PP(IX)Fe(III)Cl on the basal plane. (The edge planes of the electrode is left unmasked in order to facilitate removal of the substrate for STM measurements - see Experimental). In control experiments in which the edge planes of the HOPG electrode surface were sealed with epoxy, the apparent surface coverage of adsorbed PP(IX)Fe(III)Cl calculated from the voltammetric response was  $\sim 10$  times smaller. The higher electrochemical reactivity when the edge planes are exposed is thought to be due to the presence of highly reactive functional groups at this location. These same functional groups are not present on the basal plane except at defect sites. Thus, the STM images reported here are for films with corrected  $\Gamma$  on the order of  $10^{-10}$  mol/cm<sup>2</sup>. This later value corresponds to an average film thickness of  $\sim 3$  monolayers based on the molecular dimensions of PP(IX)Fe(III)Cl ( $\sim 14 \times 17 \text{ \AA}^2$ ) [6,8] and assuming that PP(IX)Fe(III)Cl is adsorbed in a closed-packed array with its planar face parallel to the electrode surface.

The  $0.25 \mu\text{m}^2$  STM image in Fig. 2 shows that adsorbed PP(IX)Fe(III)Cl forms a continuous film over large areas of the electrode surface. (The low magnification image of the film in Fig. 2 is representative of much larger regions of the surface) Two morphologically distinct regions of the film are apparent in Fig. 2. In the top half of the

image,  $\sim 50$  Å diameter, irregular-shaped aggregates of  $\text{PP(IX)Fe(III)Cl}$  are observed to be randomly distributed across the surface. In the lower half of the image, the film is comprised of molecular aggregates of similar size but which appear to be interconnected to form linear strands approximately 50 Å wide and of various lengths. In addition, the linear strands in the lower region are preferentially oriented ( $\sim 45^\circ$  with respect to the scan direction) suggesting either long range inter-aggregate ordering or a tip-induced ordering of aggregates. A similar ordered structure is observed in atomic force microscopy (AFM)[25,26] images of thin molecular films of  $\text{PP(IX)Fe(III)Cl}$  [27]. The structural order observed here is different than that of super-lattice structures frequently observed on bare HOPG, e.g., Moire patterns [28,29,30] and stacking faults [31]. The lower region of the image is also displaced vertically by 20 -30 Å relative to the upper region of the film, a finding that we attribute to the growth of a second layer of  $\text{PP(IX)Fe(III)Cl}$  aggregates over an underlying film or to an unseen crystallographic step on the underlying HOPG substrate. No attempt was made to determine the absolute fraction of the surface covered by the  $\text{PP(IX)Fe(III)Cl}$  film other than to note that very large regions of the surface are uniformly covered by the aggregates.

The structures observed in Fig. 2a and enlarged in Fig. 2b are consistent with the above described tendency of  $\text{PP(IX)Fe(III)Cl}$  to form large aggregates. STM images of  $\text{PP(IX)Fe(III)Cl}$  deposited at different surface coverages on HOPG reproducibly showed similar size aggregates but with varying degrees of long-range coverage. In addition to the large-area regions uniformly covered with aggregates (e.g., Fig. 2), we have also observed structures that appear to be individual aggregates and small patches of aggregates. In each case, the apparent vertical height of the aggregate or film is 10-30 Å higher than the HOPG surface.

### *Films formed by Electrooxidative Polymerization:*

Molecular films of PP(IX)Fe(III)Cl were oxidatively electropolymerized on HOPG by placing a freshly cleaved HOPG electrode in a 0.1 M sodium borate solution (pH ~10.0) containing ~0.5 mM PP(IX)Fe(III)Cl and cycling the potential between 0.0 and +1.0 V vs SCE, as shown in Fig. 3. The broad anodic peak observed when cycling the potential to +1.0 V vs SCE results from several ring centered oxidations<sup>[27]</sup>.

Oxidation of PP(IX)Fe(III)Cl at  $E_{1/2} \sim 0.36$  V produces a  $\pi$  cation radical<sup>1</sup> which can undergo radical vinyl polymerization<sup>[16,27]</sup>. Cycling the potential past this value in aqueous solutions results in the formation of an isoporphyrin species<sup>[17,32]</sup>, e.g., dioxoporphomethene<sup>[17]</sup> in the presence of nucleophiles, such as water. In this reaction, the meso positions on the porphyrin ring are replaced by hydroxy substituents to yield a dihydroxyporphyrin species which can then be further oxidized to an electrochemically-inert quinoidal dioxoporphomethene species. The decrease in the anodic peak current at 0.75 V with repetitive cycling and the concurrent decrease in the voltammetric wave at -0.52 V (corresponding to the metal centered reduction) support this mechanism. A reddish-brown film is evident on the electrode surface after cycling the electrode potential of the electrode between 0.0 and 1.0 V vs SCE. Quartz crystal microbalance studies and uv-visible spectroscopy of films prepared by oxidative polymerization of PP(IX)Fe(III)Cl quantitatively confirm the deposition of a molecular film and will be reported later<sup>[27]</sup>.

The  $0.25 \mu\text{m}^2$  STM image of a 50 nm thick film in Fig. 4(a) shows that electrooxidation of PP(IX)FeCl on HOPG forms a continuous film over large areas of the electrode surface. As seen in the image, this film is comprised of what appear to be polymer clusters of various lengths and on the order of 33 Å in width. In addition, the clusters are preferentially oriented ( $\sim 45^\circ$  with respect to the scan direction) suggesting a similar interaction of the tip with the surface and/or long range inter-aggregate ordering as

previously mention. In the top half of the image, small mounds of polymer have been deposited over the lower layer. These mounds have a vertical displacement of  $\sim 10$  Å with respect to the polymer film in the lower layer and are again oriented at  $\sim 45^\circ$  with respect to the polymer layer beneath. Essentially identical features are observed in AFM images.

Fig. 4b shows a smaller image,  $0.03 \mu\text{m}^2$ , of the same area as in Fig. 4a. This image more clearly shows the film is comprised of small oblong-shaped clusters of polymer on the order of  $\sim 40$  Å by  $\sim 80$  Å. A relatively high proportion of the clusters appear to have a deep cavity corresponding to regions of low tunneling current. We speculate that these cavities may be the interior center of coiled polymer chains, a structure that is not unexpected since the structure of the porphyrin molecule would preclude a linear structure. Another possible explanation for these cavities is that the STM tip pierces the polymer film at regions of the film which are thicker and therefore less conductive. We have previously shown, for instance, that the STM can be used to create small pinholes ( $50$  Å diameter) in thin layers of an insulating oxide ( $\text{TiO}_2$ ) deposited on a metal<sup>[33,34]</sup>. However, we note that the appearance of these structures is independent of the film thickness and voltage bias, and that they are also readily observed in AFM images<sup>[27]</sup>. These later results suggest that the STM images accurately reflect the true film structure.

### **Tunneling Spectroscopy and Analysis of the Electronic State Distribution of PP(IX)Fe(III)Cl Films.**

A key unresolved issue in STM imaging of any molecular adsorbate is the mechanism(s) of electron-transfer between the metal tip and the adsorbate-covered substrate<sup>[35,36]</sup>. Isolated individual molecules <sup>[37,38,39,40]</sup>, ordered crystalline <sup>[41,42,43,44]</sup> and semicrystalline molecular films <sup>[45,46,47]</sup>, large biomolecules <sup>[48]</sup>, organic molecular crystals <sup>[49,50]</sup>, organometallic <sup>[51]</sup> and thick conducting <sup>[52]</sup> and nonconducting

polymer films [53] have been imaged with molecular and/or near molecular resolution. In view of the rich variety of molecules that have been imaged in vacuum, air, and liquids, it appears probable that a single tunneling mechanism may not be able to account for all the observations.

Electron tunneling processes that occur during STM imaging of PP(IX)Fe(III)Cl and other electroactive molecules have, *in principle*, a similar basis as electron-transfer reactions that occur in conventional electrochemical reactions [54,55]. In the electrochemical experiment, electron-transfer occurs between a metal surface and an electroactive molecule (within a layer of solvent molecules and ions which create the electrical double layer at the solvent-substrate interface). In the STM experiment, electron-transfer occurs between a metal tip and the substrate coated with a molecular adsorbate and associated counterions. This similarity has been exploited by Morisaki and co-workers [56,57,58] in using thin SiO<sub>2</sub> tunnel barriers (on macroscopic Pt silicide substrates) in tunneling spectroscopy (TS) experiments [59] designed to probe the electronic density of states (DOS) of electrochemical molecules in solution. An important difference between the study of electron-transfer reactions in TS experiments of adsorbates and in conventional electrochemical measurements of soluble redox species is that mass-transfer limitations are expected to be absent (or less pronounced) during TS experiments due to the close proximity of the tip with the molecules and substrate. In principle, the removal of mass-transport limitations, which frequently obscure quantitative analyses of electron-transfer mechanisms, allows detailed investigations of the rates of very fast electron-transfer reactions.

Our discussion of electron transfer reactions occurring during TS is focused on electroactive molecular adsorbates that undergo chemically reversible and facile electron-transfer reactions of the type  $O + ne^- \rightleftharpoons R$  at a conducting substrate. The metal centered reduction of PP(IX)Fe(III)Cl,  $PP(IX)Fe(III)Cl + e^- \rightleftharpoons PP(IX)Fe(III)Cl^-$ ,

is a typical example of this class of reactions, undergoing a 1-e<sup>-</sup> reduction at HOPG as evidenced by the voltammetric wave shown in Fig. 1.

The tunneling current,  $I$ , in an STM experiment can be expressed as

$$I = \int_0^{eV} \rho_s(E) \rho_t(E, eV) T(E, eV) dE \quad (1)$$

where  $\rho_s(E)$  is the combined density of states of the substrate plus adsorbate (hereafter referred to as the surface distribution of states (SDOS)),  $\rho_t(E, eV)$  is the density of states of the tip in the case of a vacuum junction or the solution density of molecular states next to the electrode in the case of an electrochemical interface, and  $T(E, eV)$  is the transmission probability for electrons crossing the tunneling barrier [60]. Eq. 1 was applied as early as 1931 by Gurney [61] in establishing a quantum-mechanical basis for the non-linear electrochemical  $i$ - $V$  characteristics observed at low overpotentials (i.e., Tafel eq.). For the case of tunneling in a vacuum junction the density of states of a metallic tip,  $\rho_t(E, eV)$ , is usually taken to be nearly constant over the full range of bias voltages used [62].

The combined density of electronic states,  $\rho_s(E)$ , associated with the PP(IX)Fe(III)Cl film and HOPG electrode can be experimentally evaluated by measuring of the dependence of the tunneling current  $I$  on the voltage applied between the STM tip and electrode,  $V$ . As shown by Feenstra and coworkers [63], the SDOS associated with the tunneling process can be obtained by differentiation of eq. (1) to yield

$$\rho_s(E) \sim (dI/dV)/(I/V) \quad (2)$$

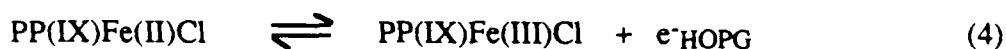
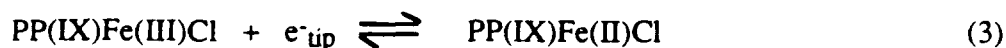
where  $(dI/dV)/(I/V)$  represents the differential conductance  $(dI/dV)$  of the tunnel junction normalized to the total or integral conductance  $(I/V)$ . The right side of eq. (2) can be

numerically evaluated from experimental I-V data to yield the SDOS associated with the adsorbate covered electrode. As theoretically and experimentally shown by others, this method of analyzing for  $\rho_s(E)$  yields tunneling spectra (i.e., plots of  $(dI/dV)/(I/V)$  vs V) that are approximately independent of the tip-to-substrate separation.<sup>[63]</sup>

To evaluate  $\rho_s(E)$  for PP(IX)Fe(III)Fe films on HOPG, we measured the tunneling current at a fixed tip-to-substrate separation as a function of V (Fig. 5a). The HOPG/PP(IX)Fe(III)Cl electrode was removed from the 0.1 M Na<sub>2</sub>B<sub>4</sub>O<sub>7</sub> solution at 0.0 V vs SCE (corresponding to the fully oxidized Fe(III) state), washed with distilled H<sub>2</sub>O and air dried. Fig. 5a shows I-V data that were obtained on the adsorbed PP(IX)Fe(III)Cl film in Fig. 2 over the area where the smaller aggregates had deposited (top of Fig. 2a). It is evident that the I-V curve has symmetric peaks about 0.0 V. In addition, the tunneling current reaches a quasi-limiting value at biases larger than  $\pm 1.0$  V. The SDOS calculated from these data are shown in Fig. 5b. Two quasi-bell shaped peaks centered at  $\pm 0.5$  eV are apparent in the TS data, representing the SDOS associated with electron tunneling processes of the HOPG/PP(IX)Fe(III)Cl structure at positive and negative biases.

For comparison, Fig. 6a and b show the I-V and  $(dI/dV)/(I/V)$ -V plots, respectively, obtained on the basal plane of bare HOPG. In contrast to the results obtained on the PP(IX)Fe(III)Cl film, the normalized conductance plot of bare HOPG shows that the density of states is described by a broad continuum with a small decrease in the SDOS near the Fermi level. The general shape of the I-V curve and SDOS for bare graphite are in agreement with previous literature reports<sup>[28]</sup>.

We propose that the general shape of SDOS plot measured for adsorbed PP(IX)Fe(III)Cl on HOPG can be accounted for by assuming that the overall electron transfer mechanism between the STM tip and the underlying HOPG substrate occurs via a charge transfer mechanism mediated by adsorbed PP(IX)Fe(III)Cl:

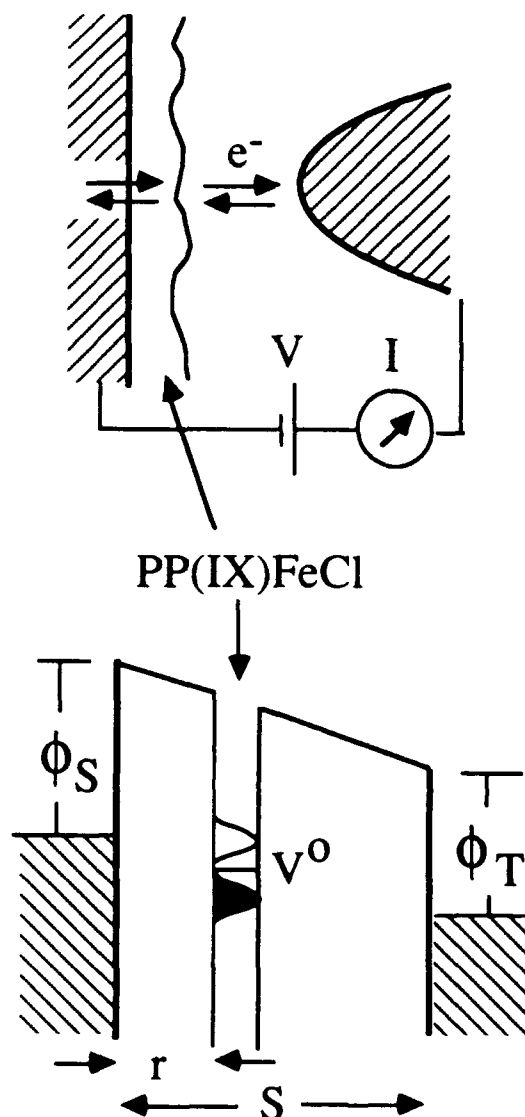


The subscripts "tip" and "HOPG" indicate the location of the transferring electron. Eqs. 3 and 4 are assumed to be reversible, allowing tunneling currents of equal magnitude to be observed at both positive and negative biases as is experimentally observed. The underlying assumption in proposing a redox mechanism (eqs. 3 and 4) is that the adsorbed PP(IX)Fe(III)Cl introduces a localized electronic state that is weakly coupled with the substrate and tip as qualitatively depicted in Scheme I. We note that a conceptually similar mechanism is implicit in recent models proposed by Gimzewski and coworkers in their analysis of the contrast in STM images of copper phthalocyanine [64] and by Zheng and Tsong in their analysis of resonant tunneling via tip-localized, molecular electron traps [65].

Assuming that electron-tunneling in the STM experiment occurs as a result of the two tunneling processes indicated in eqs. 3 and 4, the experimentally-obtained SDOS can be compared with theoretical predictions of the classical Marcus-Gerischer model which describes the polarization-dependent density of states associated with a redox couple in terms of the solvent reorganizational energy,  $\lambda$ , and the standard potential of the redox couple,  $V^0$ . In the simplest form of this theory, the density of states is given by

$$\rho_s(eV) = \Theta \exp[-(\lambda \pm e(V - V^0))^2 / (\lambda 4kT)] \quad (5)$$

where  $\Theta$  is a constant proportional to the number of electroactive species within electron-transfer distance of the electrode. The distribution function given by eq. 5 predicts that the densities of electronic states associated with the reduced and oxidized halves of an



**Scheme I.** A schematic drawing of electron-transfer reactions (*top*) between adsorbed PP(IX)Fe(III)Cl and the STM tip and HOPG substrate, and the corresponding electric potential diagram (*bottom*) showing the energy distribution of molecular redox states within the tunnel junction.

electrochemically-active molecule are described by symmetric gaussians displaced from  $V^0$  by  $\pm\lambda/e$ . The magnitude of  $\lambda$  reflects the energy associated with reorganization of the solvent upon change of the oxidation state of the molecule and with molecular structural changes, and has been the focus of numerous recent studies concerned with the dynamics of homogeneous and heterogeneous electron-transfer reactions. Morisaki and coworkers have directly evaluated  $\rho_s(\text{eV})$  for several inorganic and organic molecules through tunneling spectroscopic measurements using macroscopic electrodes and have found their results to be in good agreement with eq. 5[56,57,58].

Theoretical values of  $\rho_s(\text{eV})$  calculated from eq. 5 using  $\lambda = 0.5 \text{ eV}$  and  $V^0 = 0.0 \text{ eV}$  are shown in Fig. 5b. Comparison of the experimental SDOS with these values show that the data are in reasonable agreement with theory although a true gaussian distribution is not observed. The widths of the SDOS at the base of the curves are  $\sim 2\lambda$  in agreement with theoretical expectations.

The symmetric distribution of the experimental SDOS indicates that both oxidized (PP(IX)Fe(III)Cl) and reduced (PP(IX)Fe(II)Cl) forms of the adsorbed electroactive film participate in the tunneling processes, although only PP(IX)Fe(III)Cl is initially present in the as-formed film upon removal of the electrode from solution at 0.0 V vs SCE. This apparent inconsistency can be removed by noting that the STM tip is probing a very small absolute number of redox molecules whose redox distribution (i.e., the ratio of oxidized and reduced sites, PP(IX)Fe(III)Cl/PP(IX)Fe(II)Cl) will be affected by the sign and magnitude of the potential applied between the tip and HOPG substrate. For instance, assuming that the tip is biased at a large negative value, electrons will be transferred from the tip to PP(IX)Fe(III)Cl (eq. 3), yielding PP(IX)Fe(II)Cl which may be reoxidized (eq. 4). The magnitudes of the electron-transfer rate constants of eqs. 3 and 4 will determine which of the two intermediate tunneling steps will limit the overall flux of electrons from the tip to the substrate. Assuming that the tip-to-molecule electron transfer (eq. 3) is slow

relative to transfer between the molecule and HOPG substrate (eq. 4), the film will be comprised essentially of  $\text{PP(IX)Fe(III)Cl}$  sites, i.e.,  $\text{PP(IX)Fe(III)Cl}/\text{PP(IX)Fe(II)Cl} \gg 1$ . Conversely, at large positive tip-to-HOPG biases, electron flow will occur by the reduction of  $\text{PP(IX)Fe(III)Cl}$  via electron-tunneling from HOPG to the adsorbed layer (the reverse direction of eq. 4), followed by slow reoxidation of  $\text{PP(IX)Fe(II)Cl}$  by the tip (the reverse direction of eq. 3). Under these conditions, the molecular layer will be comprised essentially of  $\text{PP(IX)Fe(II)Cl}$  sites, i.e.,  $\text{PP(IX)Fe(III)Cl}/\text{PP(IX)Fe(II)Cl} \ll 1$ . At low positive or negative biases, the overall driving force for electron-transfer will be correspondingly smaller, and the film will be comprised of both oxidized and reduced sites. The tunneling current will be correspondingly smaller since fewer oxidized and reduced sites can serve as acceptor and donor states for electron-tunneling to the tip.

Although it is not possible to discern from our experiments whether eq. 3 or 4 is rate limiting, a similar rationalization of the symmetry of the observed SDOS can be reached by assuming that eq. 4 is the slower of the two steps. In principle, it is possible to control the rate of tunneling between the tip and adsorbed layer by varying the separation between the tip and surface. Such an experiment would unequivocally establish the relative rates of eqs. 3 and 4 and is currently being pursued in our laboratory.

The above arguments suggest that the adsorbed electroactive film, as removed from the electrochemical cell in the fully oxidized  $\text{Fe(III)}$  state, functions as both acceptor and donor states in the electron-tunneling processes, mediating the electron current between the STM tip and HOPG substrate at both positive and negative biases. The ability of one half of a redox couple to act as the charge carrying species at both positive and negative bias can be clearly demonstrated in a more conventional electrochemical experiment employing a 2-electrode thin-layer cell (TLC) [66] in which only one-half of a soluble redox couple is initially present in the solution. For example, Fig.7(a) shows the cyclic voltammetric response of a 0.4 mm radius Pt electrode (in a 3-electrode cell

arrangement) in a bulk solution of 10 mM  $\text{K}_4\text{Fe}(\text{CN})_6$  containing 0.1 M  $\text{Na}_2\text{SO}_4$  as supporting electrolyte. A voltammetric wave, centered at the half-wave potential of the  $\text{Fe}(\text{CN})_6^{3-/4}$  couple,  $E_{1/2} = 0.19$  V vs. SCE, is observed when the electrode potential is initially scanned to positive values, corresponding to the oxidation of  $\text{Fe}(\text{CN})_6^{4-}$  and re-reduction of electrogenerated  $\text{Fe}(\text{CN})_6^{3-}$  [67]. When the potential is scanned to negative values, a cathodic current at  $\sim -0.7$  V vs. SCE is observed which corresponds to the reduction of  $\text{H}_2\text{O}$  ( $E^0 = -0.66$  V vs. SCE at pH 7). When the same electrode is employed in a 2-electrode TLC as one of two identical and closely spaced plane parallel Pt electrodes (see Fig. 7), the  $i$ - $V$  behavior of the cell is a complex function of separation distance,  $d$ , between the two electrodes. At large separations,  $d = 200$   $\mu\text{m}$ , a peak-shaped  $i$ - $V$  wave is observed, Fig. 7b, that has a shape qualitatively similar to the voltammetric wave observed at an individual Pt electrode in the 3-electrode cell, Fig. 7a. However, there are two significant differences in the response. First, the wave is centered at 0.0 V applied bias (as opposed to 0.19 V in the the 3-electrode arrangement). This shift results from equilibration of the two Pt electrodes with bulk  $\text{Fe}(\text{CN})_6^{4-}$  and with the product  $\text{Fe}(\text{CN})_6^{3-}$  that is electrogenerated as current flows through the cell. It is important to realize here that the peak-shaped response does not result from the conventional oxidation and re-reduction of  $\text{Fe}(\text{CN})_6^{4-}$  at an individual electrode, as occurs in the 3-electrode arrangement employing a reference and counter electrode, Fig. 7a. Rather, the symmetric  $i$ - $V$  response results from the diffusional oxidation of  $\text{Fe}(\text{CN})_6^{4-}$  at either electrode whenever that electrode is positive with respect to the second electrode. Second, the magnitude of the peak currents are  $\sim 5$  times smaller in the 2-electrode TLC due to (i) the requirement of maintaining electroneutrality within the cell and (ii) the absence of a solution species that can be easily reduced at low potentials. In this experiment, the oxidation of  $\text{Fe}(\text{CN})_6^{4-}$  at the positive electrode must be accompanied by a cathodic process at the negative electrode. Since the most easily reduced solution species in this

experiment is  $\text{H}_2\text{O}$  (see Fig. 7a), the minimum applied bias necessary to concurrently carry out *faradaic* processes at both electrodes is equal to  $\{E^{\circ'}(\text{Fe}(\text{CN})_6^{-3/-4}) - E^{\circ'}(\text{H}_2\text{O}/\text{H}_2)\} \sim 0.9 \text{ V}$ , significantly larger than the voltage range scanned in obtaining the voltammetric response shown in Fig. 7b. Therefore, it is more probable that peak currents in the *i*-*V* response shown in Fig. 7b result from oxidation of  $\text{Fe}(\text{CN})_6^{-4}$  at the positive electrode accompanied by cathodic double layer charging of the negative electrode.

When the separation distance between the two Pt electrodes is decreased to  $\sim 10 \mu\text{m}$ , Fig. 7c, a true steady-state sigmoidally-shaped *i*-*V* response is observed which displays well-defined limiting current plateaus at both positive and negative biases. The symmetry and steady-state characteristics of this wave now reflect the fact that  $\text{Fe}(\text{CN})_6^{-4}$  oxidation at one electrode is balanced by an equal rate of  $\text{Fe}(\text{CN})_6^{-3}$  reduction at the opposite electrode.  $\text{Fe}(\text{CN})_6^{-3}$ , which is not initially present in the solution, is electrogenerated and rapidly transported across the cell gap on the slow time-scales of these measurements. The steady-state response resulting from this "feedback" mechanism is quantitatively discussed in context of twin-electrode cells employing reference and auxiliary electrodes [66b,c] and in applications of scanning electrochemical microscopy[68].

The 2-electrode TLC with only one half of a redox couple present in solution, is essentially equivalent to the STM tip/PP(IX)Fe(III)Cl/HOPG tunnel junction, with the addition of mass-transport limitations in the electrochemical cell that control the *i*-*V* response. Since the mass transport rates of  $\text{Fe}(\text{CN})_6^{-4}$  and  $\text{Fe}(\text{CN})_6^{-3}$  in the 2-electrode TLC are inversely proportional to the inter-electrode separation distance, *d*, the *i*-*V* response at sufficiently small values of *d* may eventually be limited by the heterogeneous electron-transfer reactions at the Pt electrodes (i.e.,  $\text{Fe}(\text{CN})_6^{-3} + e^- \rightleftharpoons \text{Fe}(\text{CN})_6^{-4}$ ). This point is addressed more quantitatively in a later section. The key findings of the TLC experiment are: (i) steady-state currents of exactly equal magnitudes flow through the

cell in both negative and positive biases when only one half of a reversible redox couple is present in the layer separating two closely spaced electrodes, and (ii) the Fermi-level of the two Pt electrodes and the redox potential of the solution ( $E_{1/2}$ ) are essentially equal as evidenced by the symmetry of the wave around zero bias (0.0 V). These features are observed in the TS *i*-*V* curves of for the STM tip/PP(IX)Fe(III)Cl/HOPG junction (Fig. 5a) as well as in the 2-electrode TLC with  $\text{Fe}(\text{CN})_6^{4-}$ , demonstrating the feasibility of eqs. 3 and 4 as the charge conduction mechanism in the STM experiment.

The shape of the SDOS plots suggests that the PP(IX)Fe(III)Cl molecules that comprise the electroactive film are solvated to the extent that the molecules can be reduced or oxidized. The absence of a bulk solvent in the experiment, however, prevents a detailed analysis of the significance of  $\lambda$ . The value of  $\lambda = \pm 0.5$  eV, which fit the experimental data in Fig. 5b, is well within the range of values (0.3 to 1.5 eV) measured for both inorganic and organic redox systems<sup>[69]</sup>. Although it is unlikely that a continuous film of  $\text{H}_2\text{O}$  is present on the surface after air-drying the electrodes, we speculate that the individual molecules and residual electrolyte ions ( $\text{Na}^+$  and  $\text{B}_4\text{O}_7^{2-}$ ) that comprise the film may retain their solvation shells in the absence of rigorous drying. Photoelectron spectroscopy studies of emersed electrodes, for example, clearly demonstrate that solvated ions adsorbed on metal surfaces remain intact in high vacuum<sup>[70]</sup>.

Fig. 7a and b show the *I*-*V* response and SDOS plot, respectively, for molecular films derived by oxidative electropolymerization of PP(IX)Fe(III)Cl. In contrast to the *I*-*V* curve for adsorbed PP(IX)Fe(III)Cl on HOPG, the tunneling current for this electrode increases nearly exponentially at large positive and negative biases ( $> \pm 0.75$  V), defining a region in which the current is relatively small and constant. The SDOS plot (Fig. 7b) correspondingly shows an apparent gap of  $\sim 1.5$  eV between molecular states that act as donor and acceptor levels. Analysis of the SDOS plot for this film is complicated by

mass-transport limitations that probably limit the rate of electron flow through the thicker film and by the irreversible oxidative degradation of the PP(IX)Fe(III)Cl to isoporphyrins (vide supra). The apparent bandgap observed in Fig. 7b, however, may correspond to the metal-to-ligand charge transfer of PP(IX)Fe(III)Cl which is observed in uv-visible spectra at ~610 nm or 2.03 eV[16,27]. In other studies, it has been noted that the maximum absorption for isoporphyrins occurs at ~1.0 V. It has been noted by other researchers that there is a close correspondence between the charge transfer observed spectroscopically and the difference between the half-wave potentials for oxidation and reduction of a metalloporphyrin complex<sup>[71]</sup>. The difference in the half wave potential for the reduction (-0.52 V) and first oxidation (0.36) wave of PP(IX)Fe(III)Cl is 0.88 V, similar to the band gap observed in the TS experiment. However, as noted above, the apparent SDOS for oxidatively polymerized PP(IX)Fe(III)Cl films may reflect the poor conduction in these films, rather than the properties of individual molecular species.

**Electron-Transfer Rate Constant.** While the I-V measurements do not allow identification of either eq. 3 or eq. 4 as the rate-limiting step in the tunneling mechanism, it is instructive to recast values of the tunneling current, I, as an apparent first order electron-transfer rate constant,  $k_{et}$  ( $s^{-1}$ ). This can be accomplished by defining a geometrical area of the electroactive film that encompasses the tunneling region,  $A_T$ , and using the relationship

$$I = nFA_T\Gamma(\pm V)k_{et} \quad (5)$$

In eq. (5),  $n$  is the number of electrons transferred per molecule (=1),  $F$  is the Faraday, and  $\Gamma(\pm V)$  is the bias-dependent surface density ( $mol/cm^2$ ) of electroactive molecules that can act as electron acceptors (at negative tip-to-substrate bias) and donors (at positive tip-

to-substrate bias). As discussed in the previous section, in the limit of a large applied bias,  $\Gamma(\pm V)$  is equal to the total surface coverage of electroactive molecules,  $\Gamma$ . Under these conditions, eq. (5) reduces to [67]

$$I = nFA_T\Gamma k_{et} \quad (6)$$

from which  $k_{et}(V)$  can be readily evaluated from the tunneling current and the coulometric measurement of  $\Gamma$ .

To estimate  $k_{et}$  using either eqs. (5) or (6), we assume that electron-tunneling between the tip and substrate occurs within a circular region of area  $A_T = \pi a^2$  where  $a$  is determined by the tip radius. Estimated values of the radius in the literature range from 5 - 20 Å [72] yielding  $A_T$  between 1 and  $10 \times 10^{-14}$  cm<sup>2</sup>. We assume that the electroactive film has a thickness  $d_f$  that is sufficiently thin that charge introduced into the film as a result of a redox process (eqs. 3 or 4) is removed by conduction in the direction normal to the substrate. This condition is fulfilled when  $a \gg d_f$ . For the PP(IX)Fe(III)Cl films,  $a \sim d_f \sim 10$  Å and some charge may leak outside the boundary defined by  $a$ , a complexity that we shall ignore.

Fig. 9 shows  $k_{et}$  values obtained using eq. 6 and the I-V data in Fig. 5a for an adsorbed PP(IX)Fe(III)Cl film. In calculating  $k_{et}$ , we assume  $\Gamma$  is equal to the electrochemically measured surface coverage ( $10^{-10}$  mol/cm<sup>2</sup>) and  $a = 10$  Å. The data in Fig. 9 show that  $k_{et}$  increases from  $\sim 10^9$  s<sup>-1</sup> at zero bias ( $V = 0$ ) to  $\sim 5 \times 10^{10}$  s<sup>-1</sup> at large positive or negative bias,  $|V| \geq 0.7$  V. The dependence of  $k_{et}$  on  $V$  can be attributed to either a decrease in the activation energy for electron-transfer (eqs. 3 and 4) at large biases, or to an increase in the number of molecules that can act as donor and acceptor states at large positive and negative biases, respectively. As previously discussed, at low biases, the electroactive film will be comprised of both oxidized and reduced sites and eq.

6, which is based on the voltage-dependent number of acceptor and donor states,  $\Gamma(\pm V)$ , is clearly a more appropriate equation. To determine the functional dependence of  $\Gamma(\pm V)$ , however, would require a detailed kinetic model that relates  $k_{et}$  to the local electric potential,  $\phi(x)$ , within the tunneling junction (see Scheme I). Since  $\phi(x)$  is not known, the variation of  $\Gamma(\pm V)$  with applied bias can not be readily determined. However, the symmetry of the I-V response suggests that an approximately equal number of reduced and oxidized molecules at low biases exist in the region of the film that comprises the tunnel junction. Thus,  $\Gamma(\pm V)$  varies from  $\sim 1/2\Gamma$  at low bias to  $\Gamma$  at  $|V| \geq 0.7$  V. The use of eq. 5 and  $\Gamma$  thus introduces a small error (factor of  $\sim 2$ ) in  $k_{et}$  at low bias. The nearly 50-fold increase in  $k_{et}$  with increasing bias thus probably reflects a lowering of the activation energy for electron-tunneling.

The observed dependence of  $k_{et}$  on  $V$  closely resembles the functional dependence of homogeneous electron-transfer rate constants on reaction free energy change ( $\Delta G^0$ )<sup>[73]</sup>. Because of the complex potential distribution within the tunnel region, however, the applied bias is not necessarily equal to  $\Delta G^0$  nor can it be ascertained if a strict linear proportionality exists between the two quantities. However, since it is obvious that the driving force for electron transfer increases with increasing bias, Fig. 9 is indeed a qualitative form of a free energy correlation.

As a final comment, in an alternative analysis of the I-V response, we have considered the effects of diffusional electron conduction within PP(IX)Fe(III)Cl films. Electron-transport in multilayer polymer films occurs by self-exchange electron-transfer reactions between reduced and oxidized sites which are accurately modeled as a diffusional flux of electrons<sup>[74]</sup>. For a film of thickness  $d_f$  and cross-sectional area  $A_T$ , the maximum diffusional flux is given by

$$I = nFA_T D_e \Gamma / d_f^2 \quad (7)$$

where  $D_{e^-}$  is an apparent diffusion coefficient for electrons and the other symbols represent previously defined quantities. Using the maximum current of  $I$  in Fig. 5a,  $d_f = 20 \text{ \AA}$ , and  $A_T = 3.1 \times 10^{-14}$  yields  $D_{e^-} = 10^{-2} \text{ cm}^2/\text{s}$ . Since this value is  $\sim 10^4$  times larger than the largest diffusion constants reported for electron conduction in redox films<sup>[75]</sup>, we have not pursued this direction of analysis.

## CONCLUSION.

The experimental investigations presented here suggest that STM and TS can be used to probe the electronic, as well as topographic, structure of electroactive molecular films. Our preliminary analysis of electron-tunneling mechanism suggests that the redox reactions of PP(IX)Fe(III)Cl films mediate the flux of electrons between the STM tip and substrate. This conclusion is based on the similarity of the measured SDOS with Marcus-Gerischer theory that describes the distribution of states for electroactive molecules.

Our study has also demonstrated that electrochemical responses of electroactive films are paralleled by the behavior observed in TS experiments. Specifically, electron-transfer reactions appear more facile in both electrochemical and TS measurements for adsorbed PP(IX)Fe(III)Cl films than for films derived by oxidative polymerization of PP(IX)Fe(III)Cl.

It is interesting to note that the measured values of  $k_{et}$  ( $10^9 - 5 \times 10^{10} \text{ s}^{-1}$ ) obtained in the tunneling measurements are of the same order of magnitude as recently reported values of the first-order rate constants for exothermic electron-transfer reactions between dissimilar electroactive molecules separated by a saturated hydrocarbon spacer. For instance, Jordan et al. obtained  $k_{et}$  values as large as  $1.8 \times 10^{10} \text{ s}^{-1}$  from time-resolved fluorescence measurements for excited-state electron-transfer from zinc meso-phenyloctamethylporphyrin to a series of benzoquinones separated by a  $10 \text{ \AA}$  long rigid hydrocarbon spacer<sup>[76]</sup>. Similar experiments by Closs and Miller yielded comparable

values of electron-transfer rate constants ( $10^9 - 10^{10} \text{ s}^{-1}$ ) for rigidly spaced electron donor and acceptor pairs<sup>[77]</sup>. Although obvious physical and chemical differences exist between the mechanisms of electron transfer involved in the STM experiment and in the purely chemical systems, the conceptual similarity between these reactions and the order-of-magnitude agreement in the observed rates suggests that STM can be employed to investigate the dynamics of extremely fast electron transfer reactions. We are currently pursuing this area of research.

#### **ACKNOWLEDGEMENTS.**

The authors gratefully acknowledge insight provided in discussions with Silvia Lopez, Michael Ward, Hector Abruna, and L.A. Bottomley, and the assistance of E. R. Scott in preliminary TLC experiments. This work was supported by the Office of Naval Research. STM facilities were supported by the Center for Interfacial Engineering with funding from the NSF Engineering Research Centers Program (CDR 8721551) and industrial sponsors.

## REFERENCES

---

1. Fuhrhop, J.H. *Structure and Bonding*; Dunitz, J.D.; Hemmerich, P.; Holm, R.H.; Ibero, J.A.; Jorgensen, C.K.; Neilands, J.B.; Reinen, D.; Williams, R.J.P., Eds.; Springer-Verlag: New York, N.Y.; 1974; Vol. 18, p 1.
2. Felton, R.H. *The Porphyrins*; Dolphin, D., Ed.; Academic Press: New York, N.Y., 1978; Vol. V.
3. Maler, H.R. and Cordes E.H. *Biological Chemistry* 2nd ed.; Harper and Row: New York, N.Y., 1971; Ch. 15.
4. (a) Wan, G.X.; Shigehara, K.; Tsuchida E.; Anson, F.C. *J. Electroanal. Chem.* **1984**, 179, 239. (b) Shigehara K.; Anson, F.C. *J. Phys. Chem.* **1982**, 86, 2776. (c) Meyer G.; Savy, M. *Electrochim. Acta* **1977**, 22, 213. (d) Collman J.P.; Denisovich, P.; Konai, Y.; Marrocco, M.; Koval, C.; Anson, F.C. *J. Am. Chem. Soc.* **1980**, 102, 6027. (e) Collman, J.P.; Hendricks, N.H.; Leidner, C.R.; Ngameni, E.; L'Her, M. *Inorg. Chem.* **1988**, 27, 387. (f) Kadish, K.M.; Rhode, R.K.; Shiue, L.R.; Bottomley, L.A. *Inorg. Chem.* **1981**, 20, 1274. (g) Sawaguchi, T.; Itabashi, T.; Matsue, T.; Uchida, I. *J. Electroanal. Chem.* **1990**, 279, 219. (h) Tieman, R.S.; Coury, L.A. Jr.; Kirchoff, J.R.; Heineman, W.R. *J. Electroanal. Chem.* **1990**, 281, 133. (i) Jiang, R.; Dong, S. *J. Electroanal. Chem.* **1990**, 291, 11. (j) Su, Y.O.; Kuwana, T.; Chen, S. *J. Electroanal. Chem.* **1990**, 288, 177. (k) Collman, J.P.; Kim, K. *J. Am. Chem. Soc.* **1986**, 108, 7847. (l) Collman, J.P.; Anson, F.C.; Barnes, C.E.; Bencosme, C.E.; Geiger, T.; Evitt, E.R.; Kreh, R.P.; Meier, K.; Pettman, R.B. *J. Am. Chem. Soc.* **1983**, 105, 2694. (m) Durand, R.R. Jr.; Bencosme, C.S.; Collman, J.P.; Anson, F.C. *J. Am. Chem. Soc.* **1983**, 105, 2710. (n) James, B.R. *The Porphyrins*; Dolphin, D., Ed.; Academic Press: New York, N.Y., 1978; Vol. V, Ch. 6.

- 
5. (a) Kadish, K.M.; Larson, G.; Lexa, D.; Momenteau, M. *J. Am. Chem. Soc.* **1975**, *97*, 282. (b) Kadish, K.M.; Jordan, J. *J. Electrochem. Soc.* **1978**, *125*, 1250. (c) Kadish, K.M.; Morrison, M.M.; Constant, L.A.; Dickens, L.; Davis, D.G. *J. Am. Chem. Soc.* **1976**, *98*, 8387. (d) Kaaret, T.W.; Zhang, G.; Bruice, T.C. *J. Am. Chem. Soc.* **1991**, *113*, 4652. (e) Davis, D.G.; Bynum, L.M. *Bioelectrochem. Bioenerget.* **1975**, *2*, 184.
  6. Bianco, P.; Haladjian, J.; Draoui, K. *J. Electroanal. Chem.* **1990**, *279*, 305.
  7. Brown, A.P.; Koval, C.; Anson, F.C. *J. Electroanal. Chem.* **1976**, *72*, 379.
  8. Kolpin, C.F.; Swofford, H.S. Jr. *Anal. Chem.* **1978**, *50*, 916.
  9. Alben, J.O.; Fuchsman, W.H.; Beardreau, C.A.; Caughey, W.S. *Biochemistry* **1968**, *7*, 624..
  10. Binnig, G.; Rohrer, H.; Gerber, Ch.; Weibel, E. *Phys. Rev. Lett.* **1982**, *49*, 57.
  11. Binnig, G.; Rohrer, H. *Hel. Phys. Acta* **1982**, *55*, 726.
  12. Marcus, R.A. *J. Chem. Phys.* **1956**, *24*, 966.
  13. Gerischer, H. *Z. Phys. Chem. N. F.* **1961**, *27*, 48.
  14. Levich, V. G. *Adv. Electrochem. Electrochem. Eng.* **1966**, *4*, 249.
  15. Morrison, S. R. *Electrochemistry at Semiconductor and Oxidized Metal Electrodes*; Plenum Press: New York, 1980; and references therein.
  16. Macor, K.A.; Spiro, T.G. *J. Am. Chem. Soc.* **1983**, *105*, 5601.
  17. Macor, K.A.; Spiro, T.G. *J. Electroanal. Chem.* **1984**, *163*, 223.
  18. Medhi, O.K.; Silver, J. *Inorganica Chimica Acta* **1988**, *153*, 133.
  19. White, W.I. *The Porphyrins*; Dolphin, D., Ed.; Academic Press: New York, N.Y., 1978; Vol. V, Ch. 7.
  20. Haurowitz, F. *Hoppe-Seyler's Z. Physiol. Chem.* **1938**, *254*, 266.
  21. Blauer, G.; Zvilichovsky, B. *Arch. Biochem. Biophys.* **1968**, *127*, 749.

- 
22. Shack, J.; Clark, W.M. *J. Biol. Chem.* **1947**, 171, 143.
23. (a) Gallagher, W.A.; Elliot, W.B. *Ann. N.Y. Acad. Sci.* **1973**, 206, 463.(b)  
Jones, P.; Prudhoe, K.; Brown, S.B. *J. Chem Soc. Dalton Trans.* **1974**, 911 (c)  
Makinen, M. W.; Eaton, W.A. *Ann. N.Y. Acad. Sci.* **1973**, 206, 210.
24. Lemberg, R.; Legge, J.W. *Hematin Compounds and Bile Pigments*; Wiley  
(Interscience): New York, 1979.
25. Binnig, G.; Gerber, Ch.; Stoll, E.; Albrecht, T.R.; Quate, C.F. *Surf. Sci.* **1987**,  
189, 1.
26. Manne, S.; Hansma, P.K.; Massie, J.; Elings, V.B.; Gewirth, A.A. *Science* **1991**,  
251, 183.
27. Snyder, S.; Lopez, S.; White, H.S. to be submitted to *J. Am. Chem. Soc.* **1991**.
28. Kuwabara, M.; Clarke, D. R.; Smith, D. A. *Appl. Phys. Lett.* **1990**, 56, 2396.
29. Womelsdorf, J. F.; Ermler, W. C.; Sandroff, C. J. *J. Phys. Chem.* **1991**, 95, 503.
30. Liu, C.; Chang, H.; Bard, A. J. *Langmuir* **1991**, 7(6), 1138.
31. Snyder, S.; Foecke, T.; White, H. S.; Gerberich, W. W. *J.Mats. Res.*, in press.
32. (a) Dolphin, D.; Felton, R.H.; Borg, D.C.; Fajer, J. *J. Amer. Chem. Soc.* **1970**,  
92, 743. (b) Kadish, K.M.; Rhodes, R.K. *Inorg. Chem.* **1981**, 20, 2691. (c) Su,  
Y.O.; Kim, D.; Spiro, T.G. *J. Electroanal. Chem.* **1988**, 246, 363.
33. Casillas, N.; Snyder, S.R.; White, H.S. *J. Electrochem. Soc.* **1991**, 138, 641.
34. Casillas, N.; Snyder, S.R.; Smyrl, W.; White, H.S. *J. Phys. Chem.* **1991**, 95,  
7002.
35. Spong, J.K.; Mizes, H.A.; LaComb, L.J.; Dovek, M.M.; Frommer, J.E.; Foster,  
J.S. *Nature* **1989**, 338, 137.
36. Mizutani, W.; Shigeno, M.; Ono, M.; Kajimura, K. *Appl. Phys. Lett.* **1990**, 56,  
1974.

- 
37. Lippel, P.H.; Wilson, R.J.; Miller, M.D.; Woll, Ch.; Chiang, S. *Phys. Rev. Lett.* **1989**, 62, 171.
  38. Schardt, B. C.; Yau, S.; Rinaldi, F. *Science* **1989**, 243, 1050.
  39. Ohtani, H.; Wilson, R.J.; Chiang, S.; Mate, C.M. *Phys. Rev. Lett.* **1988**, 60, 2398.
  40. Moller, R.; Coenen, R.; Esslinger, A.; Koslowski, B. *J. Vac. Sci. Technol. A* **1990**, 8, 659.
  41. Smith, D.P.E.; Horber, H.; Gerber, Ch.; Binnig, G. *Science* **1989**, 245, 43.
  42. Foster, J.S.; Frommer, J.E. *Nature* **1988**, 333, 542.
  43. Michel, B.; Travaglini, G.; Rohrer, H.; Joachim, C.; Amrein, M. *Z. Phys. B.* **1989**, 76, 99.
  44. Mizutani, W.; Shigeno, M.; Sakakibara, Y.; Kajimura, K.; Ono, M.; Tanishima, S.; Ohno, K.; Tushima, N. *J. Vac. Sci. Technol. A* **1990**, 8, 675.
  45. McGonigal, G.C.; Bernhardt, R. H.; Thomson, D.J. *Appl. Phys. Lett.* **1990**, 57, 28.
  46. Smith, D.P.E.; Kirk, M.D.; Quate, C.F. *J. Chem. Phys.* **1987**, 86, 6034.
  47. Wu, X.; Lieber, C.M. *J. Phys. Chem.* **1988**, 92, 5556.
  48. Amrein, M.; Stasiak, A.; Gross, H.; Stoll, E.; Travaglini, G. *Science* **1988**, 240, 514.
  49. Sleator T.; Tycko, R. *Phys. Rev. Lett.* **1988**, 60, 1418.
  50. Widrig, C.A.; Alves, C.A.; Porter, M.D. *J. Am. Chem. Soc.* **1991**, 113, 2805.
  51. Lyding, J.W.; Hubacek, J.S.; Gammie, G.; Skala, S.; Brockenbrough, R.; Shapley, J.R.; Keles, M.P. *J. Vac. Sci. Technol. A* **1988**, 6, 363.
  52. Yang, R.; Dalsin, K.M.; Evans, F.; Christensen, L.; Hendrickson, W.A. *J. Phys. Chem.* **1989**, 93, 511.

- 
53. Snyder, S.R.; White, H.S.; Lopez, S.; Abruna, H.D. *J. Am. Chem. Soc.* **1990**, 112, 1333.
54. Sass, J. K.; Gimzewski, J. K. *J. Electroanal. Chem.* **1988**, 251, 241.
55. Travaglini, G.; Amrein, M.; Michel, B.; Gross, H. *Scanning Tunneling Microscopy and Related Methods*; Behm, R.J.; Garcia, N.; Rohrer, H., Eds.; Kluwer Academic Publishers: Netherlands, 1990; p 335.
56. Morisaki, H.; Nishikawa, A.; Ono, H.; Yazawa, K. *J. Electrochem. Soc.* **1990**, 137, 2759.
57. Morisaki, H.; Ono, H.; Yazawa, K. *J. Electrochem. Soc.* **1989**, 136, 1710.
58. Morisaki, H.; Ono, H.; Yazawa, K. *J. Electrochem. Soc.* **1988**, 135, 381.
59. Bennett, A. *J. Electroanal. Chem.* **1975**, 60, 125.
60. Giaever, I. *Phys. Rev. Lett.* **1960**, 5, 464.
61. Gurney, R.W. *Proc. Royal Soc. (London)* **1932**, 134A, 137.
62. Park, S.; Nogami, J.; Mizes, H.A.; Quate, C.F. *Phys. Rev. B* **1988**, 38, 4269.
63. Feenstra, R.M.; Stroscio, J.A.; Fein, A.P. *Surf. Sci.* **1987**, 181, 295.
64. Gimzewski, J.K.; Stoll, E.; Schlittler, R.R. *Surf. Sci.* **1987**, 181, 267.
65. Zheng, N.J.; Tsong, I.S.T. *Phys. Rev. B* **1990**, 40, 2671.
66. (a) Hubbard, A.T.; Anson, F.C. *The Theory and Practice of Electrochemistry in Thin Layer Cells - Electroanalytical Chemistry*; Bard, A.J., Ed.; Marcel Dekker: N.Y., 1970; Vol. 4. (b) Anderson, L. B.; Reilley, C.N. *J. of Electroanal. Chem.* **1965**, 295, 205. (c) Reilley, C.N. *Rev. Pure and Appl. Chem.* **1968**, 18, 137. (d) Bard, A.J.; Faulkner, L.R. *Electrochemical Methods: Fundamentals and Applications*; John Wiley & Sons, Inc.: 1980; Ch. 14.
67. Bard, A.J.; Faulkner, L.R. *Electrochemical Methods: Fundamentals and Applications*; John Wiley & Sons, Inc.: 1980; Ch. 12.

- 
68. (a) Kwak, J.; Bard, A.J. *Anal. Chem.* **1989**, 61, 1221. (b) Wipf D.O.; Bard, A.J. *J. Electrochem. Soc.* **1991**, 138(2), 469. (c) Lee, C.; Bard, A.J. *Anal. Chem.* **1990**, 62, 1906. (d) Scott, E.R.; White, H.S. *J. of Membrane Sci.* **1991**, 58, 71. (d)Hansma, P.K.; Drake, B.; Marti, O.; Gould, S.A.C.; Prater, C.B. *Science* **1989**, 243, 641.
69. Morisaki, H.; Ono, H.; Yazawa, K. *Photoelectrochemistry and Electrosynthesis on Semiconducting Materials*; Ginley, D.S.; Honda, K.; Nozik, A.; Fujishima, A.; Armstrong, N.; Sakata, T.; Kawai, T., Eds.; The Electrochemical Society Softbound Proceedings Series: Pennington, N.J., 1988; Vol. 88-14, p 436.
70. (a) Yeager, E. *Surf. Sci.* **1980**, 101, 1. (b) Neff, H.; Foditsch, W.; Kotz, R. *J. of Electron Spec. and Related Phenomena* **1984**, 33, 171. (c) Kotz, E.R.; Neff H.; Muller, K. *J. Electroanal. Chem.* **1986**, 215, 331. (d)Rath, D.L.; Kolb, D.M. *Surf. Sci.* **1981**, 109, 641. (e) Hansen, W.N.; Kolb, D.M.; Rath D.L.; Wille, R. *J. Electroanal. Chem.* **1980**, 110, 369.
71. Makinen, M.W.; Churg A.K. *Iron Porphyrins-Part One*; Lever, A.B.P.; Gray, H.B., Eds.; Physical Bioinorganic Chemistry Series, Addison-Wesley Publishing Company: 1983; Ch. 3.
72. Behm, R.J. *Scanning Tunneling Microscopy and Related Methods*; Behm, R.J.; Garcia, N.; Rohrer, H., Eds.; Kluwer Academic Publishers: 1989; p 173.
73. (a) Ballardini, R.; Varani, G.; Indelli, M.T.; Scandola, F.; Balzani, V. *J. Am. Chem. Soc.* **1978**, 100, 7219. (b) Rehm, D.; Weller, A. *Isr. J. Chem.* **1970**, 8, 259.
74. (a) Dalton, E.F.; Murray, R.W. *J. Phys. Chem.* **1991**, 95, 6383. (b) Shu, C.F.; Wrighton, M.S. *J. Phys. Chem.* **1988**, 92, 5221. (c) Buttry, D.A.; Anson, F.C. *J. Am. Chem. Soc.* **1983**, 105, 685. (d) Jernigan, J.C.; Surridge, N.A.; Zvanut,

- 
- M.E.; Silver, M.; Murray, R.W. *J. Phys. Chem.* **1989**, 93, 4620. (e) Andrieux, C.P.; Saveant, J.M. *J. Electroanal. Chem.* **1980**, 111, 377. (f) Dahms, H.J. *J. Phys. Chem.* **1968**, 72, 362. (g) Ruff, I. *Electrochim. Acta* **1970**, 15, 1059. (h) Ruff, I.; Botar, L. *J. Chem. Phys.* **1985**, 83, 1292. (i) Ruff, I.; Friedrich, V.J. *J. Phys. Chem.* **1971**, 75, 3297 and 3303.
75. Murray, R.W. *Electroanalytical Chemistry*; Bard, A.J., Ed.; Wiley: N.Y., 1984; Vol. 14.
76. Joran, A.D.; Leland, B.A.; Felker, P.M.; Zewall, A.H.; Hopfield, J.J.; Dervan, P.B. *Nature* **1987**, 327, 508.
77. Closs, G.L.; Miller, J.R. *J. Am. Chem. Soc.* **1984**, 106, 3047.

## FIGURES.

1. Cyclic voltammetric response of a HOPG/PP(IX)Fe(III)Cl (adsorbed) electrode in a  $N_2$ -purged, 0.1 M  $Na_2B_4O_7$  solution. Voltammetric sweep rate = 50 mV/sec.
2. STM image of an HOPG/PP(IX)Fe(III)Cl (adsorbed) electrode: (a) 500 x 500 nm image; (b) 175 x 175 nm enlargement of (a) ( $V_t = 0.1$  V;  $i_t = 1.2$  nA).
3. Cyclic voltammetric response of a HOPG electrode in a  $N_2$ -purged, 0.1 M  $Na_2B_4O_7$  solution containing 0.5 mM PP(IX)Fe(III)Cl. Voltammetric sweep rate = 50 mV/sec. Successive scans show a decrease in both the anodic peak current at 0.75 V and the voltammetric wave at -0.52 V vs SCE.
4. STM image of an HOPG electrode after potential cycling between 0.0 and +1.0 vs SCE in 0.1 M  $Na_2B_4O_7$  solution containing 0.5 mM PP(IX)Fe(III)Cl. (a) 500 x 500 nm image ( $V_t = -224$  mV;  $i_t = 0.54$  nA). (b) 180 x 180 nm image ( $V_t = -100$  mV;  $i_t = 1.00$  nA).
5. (a) I-V curve for a HOPG/PP(IX)Fe(III)Cl (adsorbed) electrode. (b) SDOS plot  $((dI/dV)/(I/V) \text{ vs } (V))$  of the HOPG/PP(IX)Fe(III)Cl (adsorbed) electrode from the data in (a) are shown as circles (o). The theoretical SDOS (solid line) is calculated from eq. (5) in the text.
6. (a) I-V curve for a bare HOPG electrode. (b) SDOS plot  $((dI/dV)/(I/V) \text{ vs } (V))$  of the data in (a).

7. (a) Cyclic voltammetric response in 0.01 M  $\text{K}_4\text{Fe}(\text{CN})_6$  and 0.1 M  $\text{Na}_2\text{SO}_4$  of a Pt electrode (0.4 mm radius) in a 3-electrode cell containing a SCE reference and Pt auxiliary electrodes. I-V response of a 2-electrode thin-layer cell comprised of two identical Pt electrodes separated by (b) 200  $\mu\text{m}$  and (c) 10  $\mu\text{m}$  and containing the same solution as in (a). Scan rate: 100 mV/s. In (a), V is measured vs. the SCE. In (b) and (c), V is the applied bias between the two Pt electrodes.
8. (a) I-V curve for an HOPG electrode after anodic electropolymerization of  $\text{PP}(\text{IX})\text{Fe}(\text{III})\text{Cl}$ . (b) SDOS plot  $((dI/dV)/(I/V))$  vs (V) calculated from the data in (a).
9. Plot of electron-transfer rate constant ( $k_{\text{et}}$ ,  $\text{s}^{-1}$ ) as a function of the total potential applied between the STM tip and HOPG/ $\text{PP}(\text{IX})\text{Fe}(\text{III})\text{Cl}$  (adsorbed) electrode.  $k_{\text{et}}$  values are calculated from tunneling currents, I, using eq. (6) in the text. Open (o) and closed circles (•) represent values measured at negative and positive biases (sample vs. tip), respectively

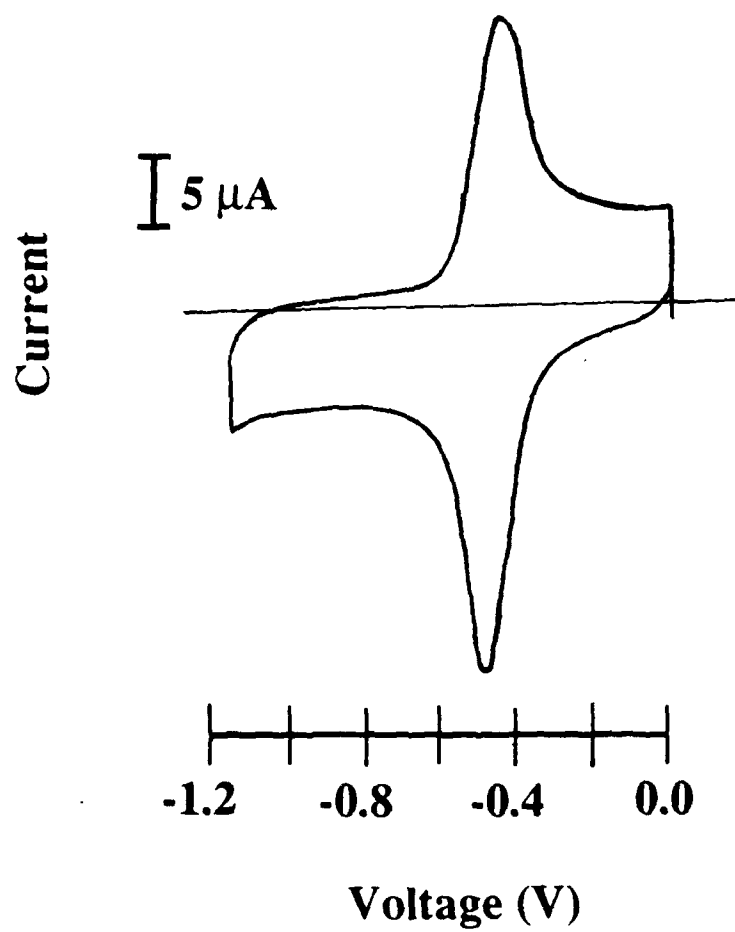
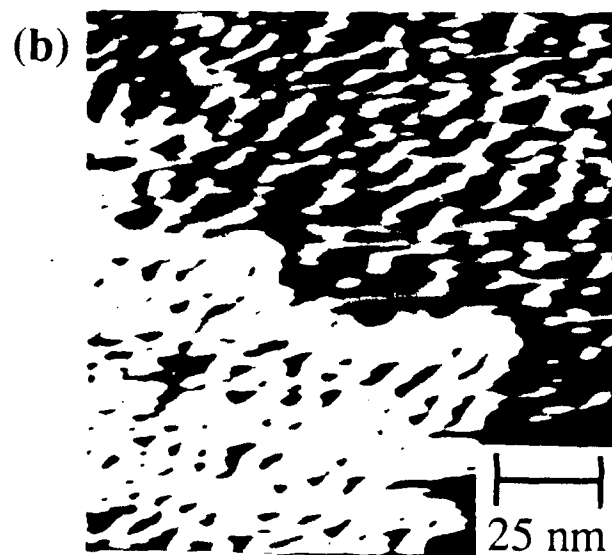
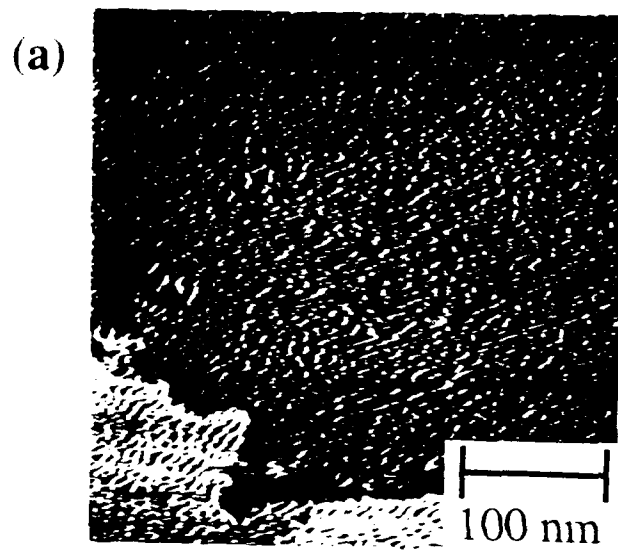


Fig. 1



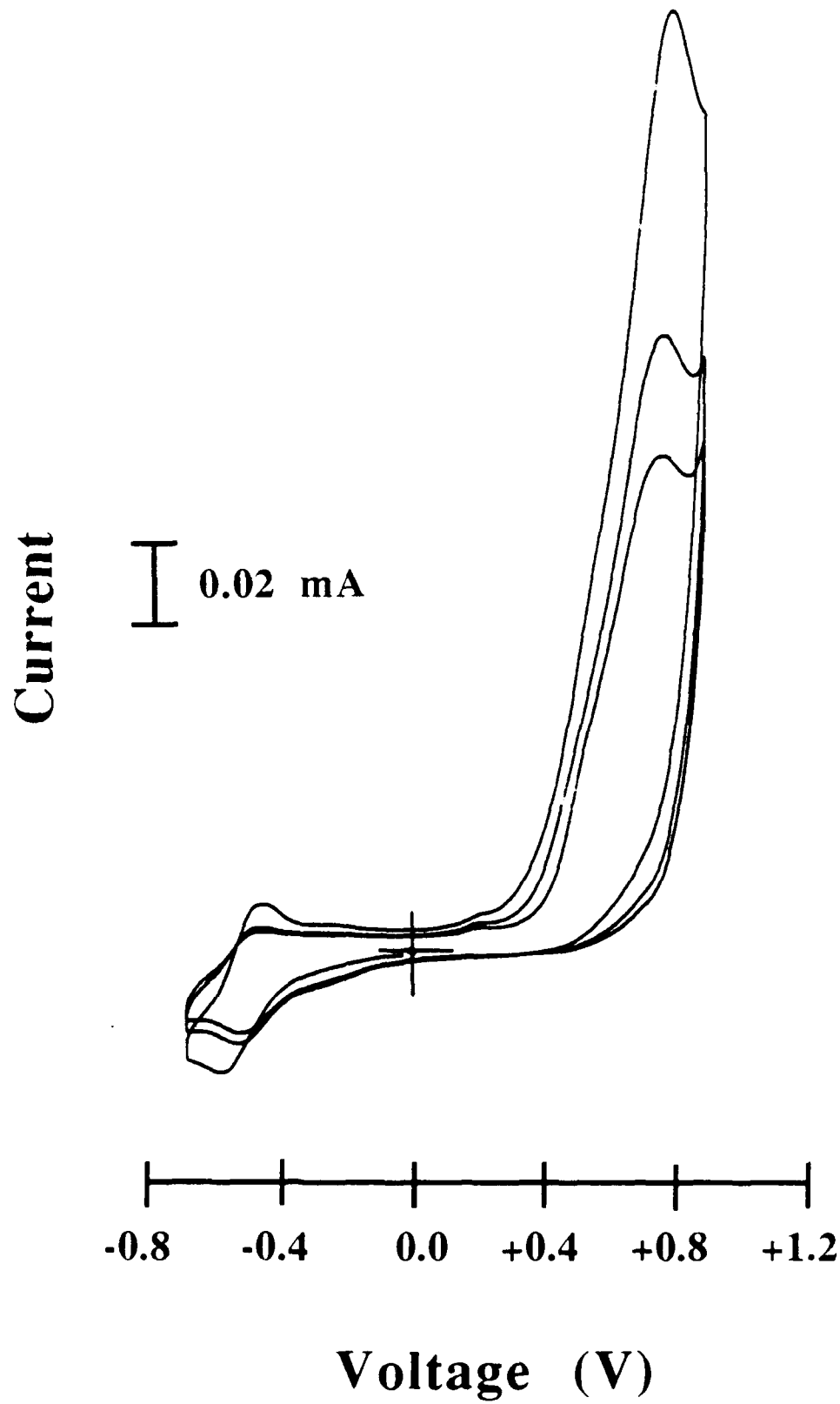
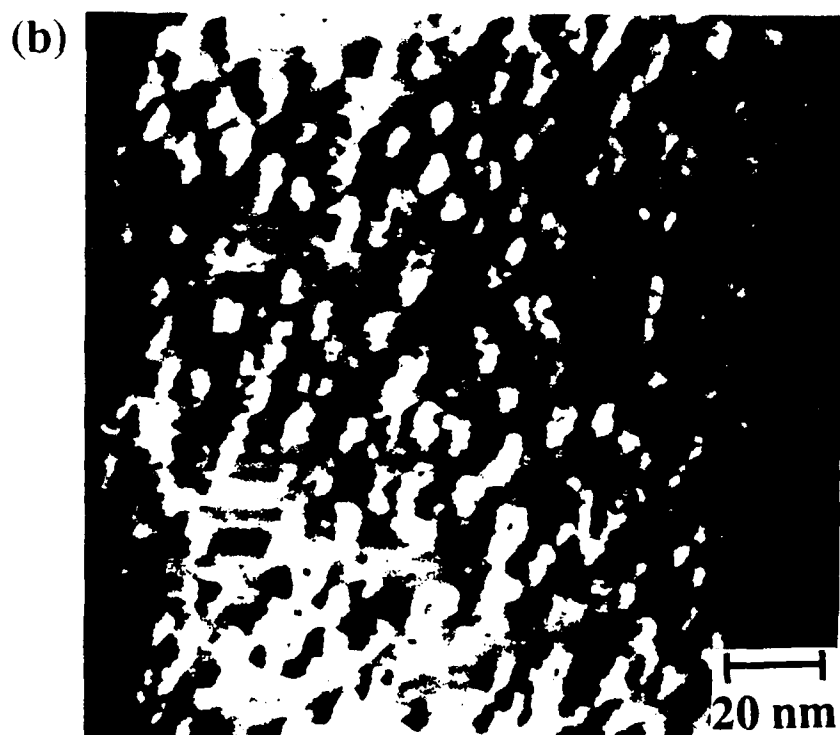
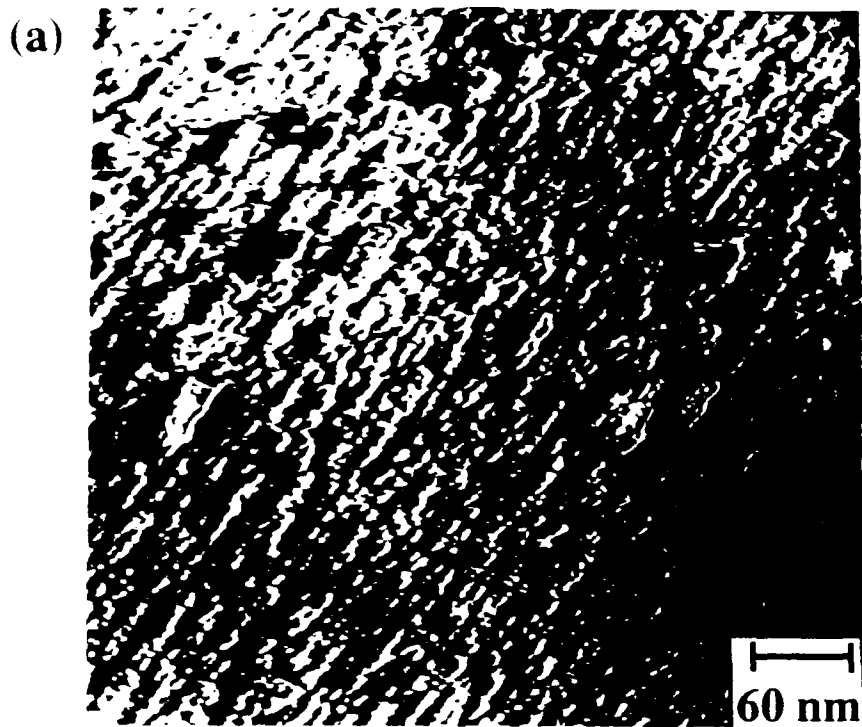
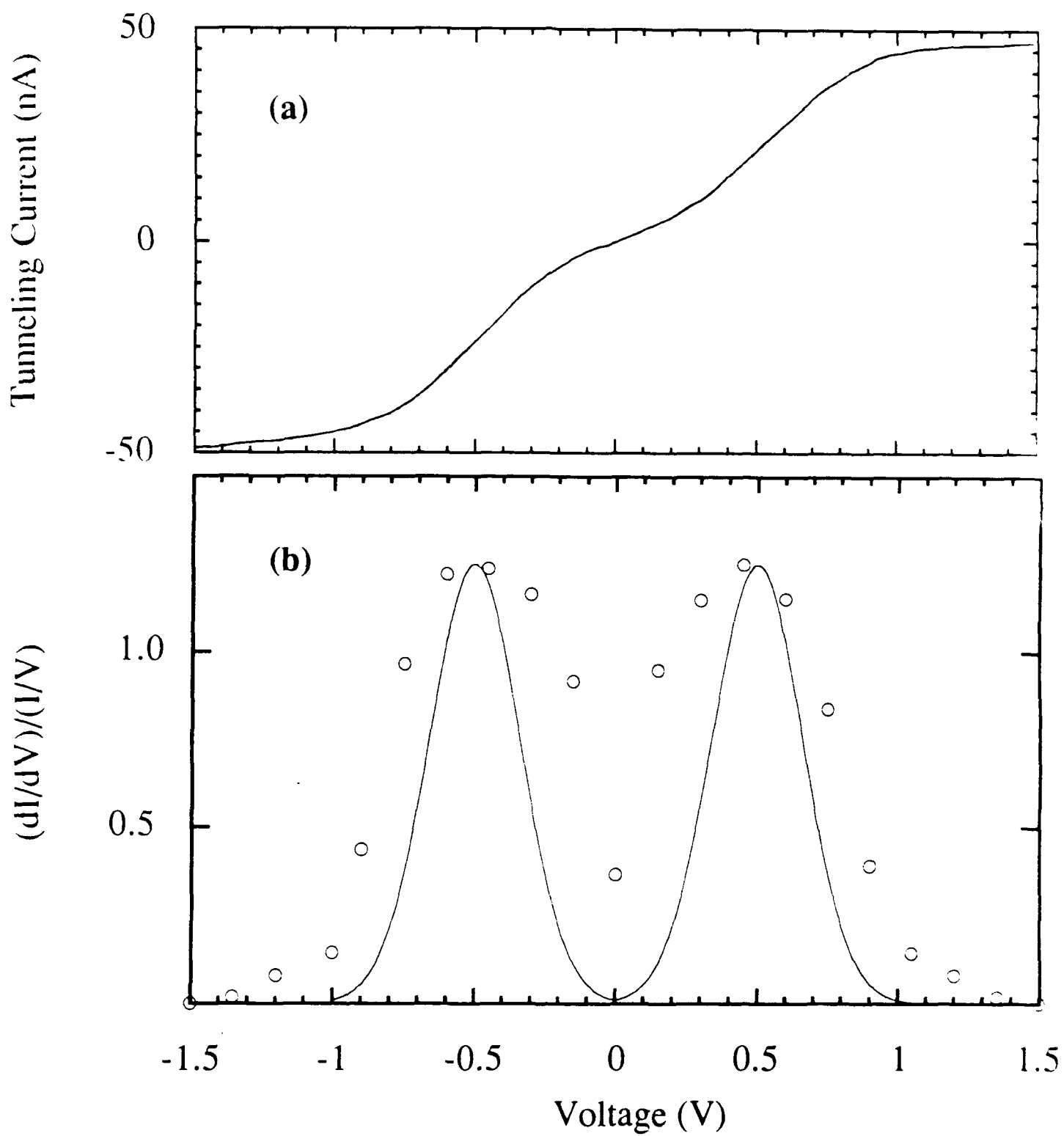


Fig. 3





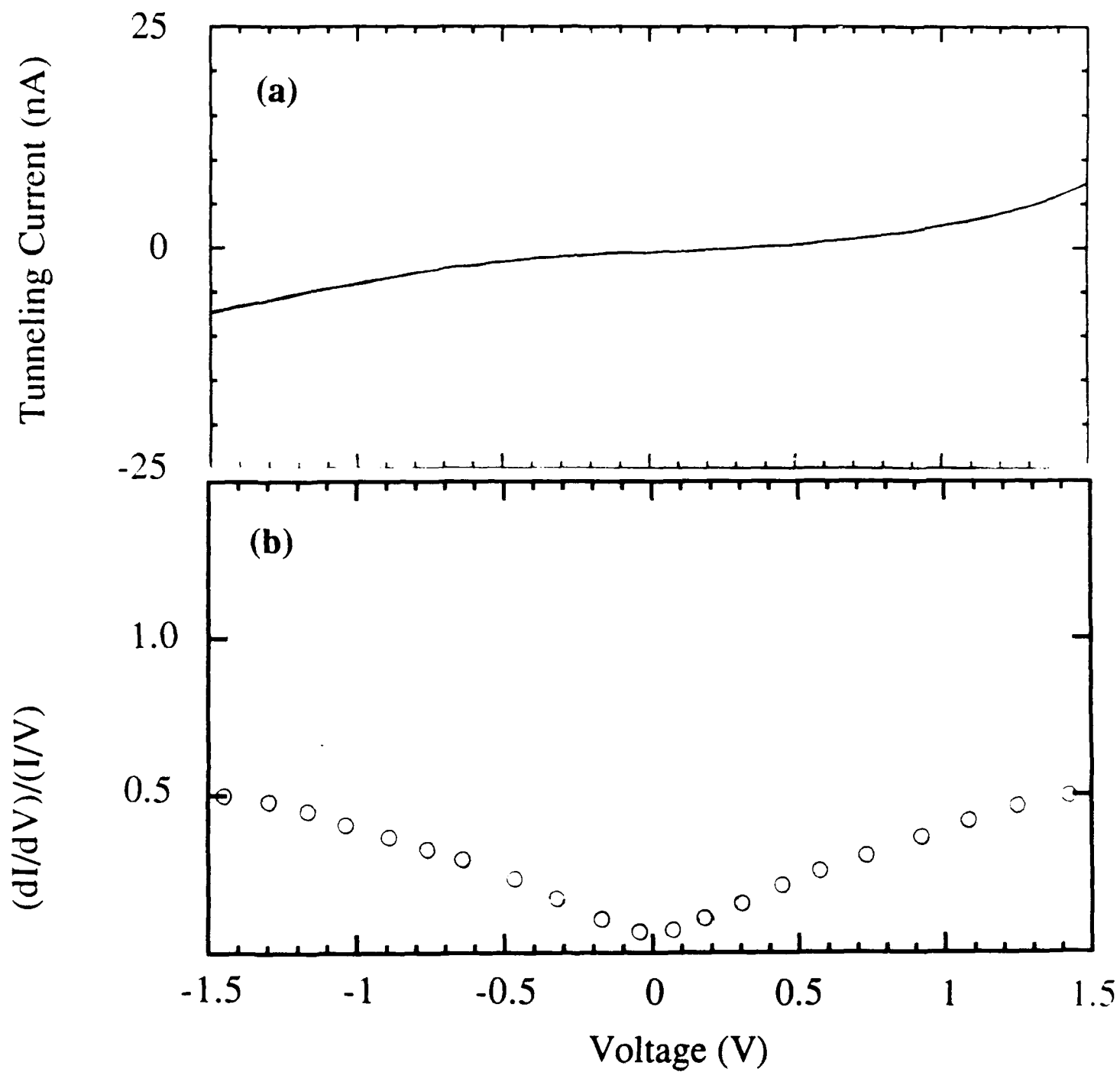
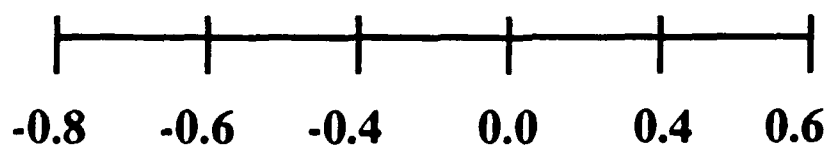
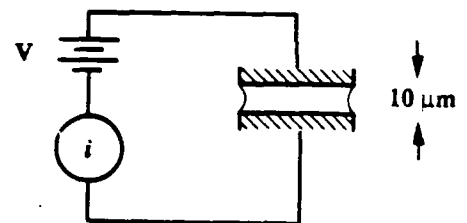
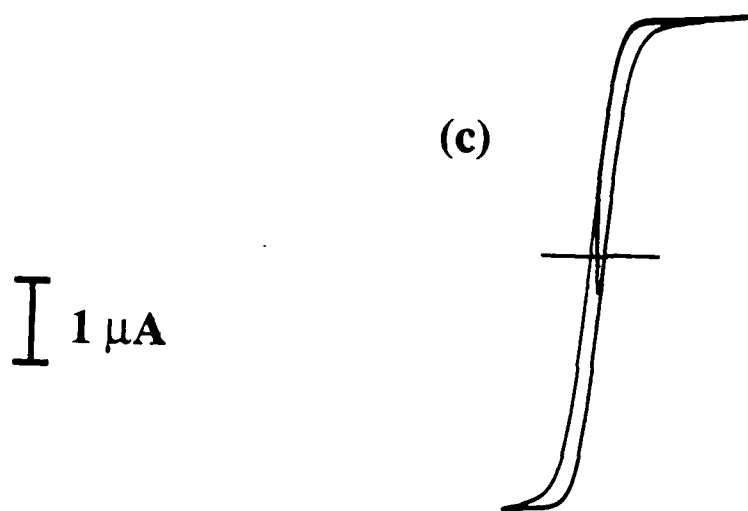
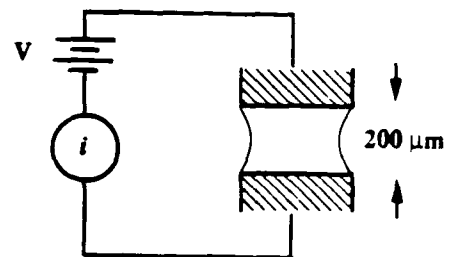
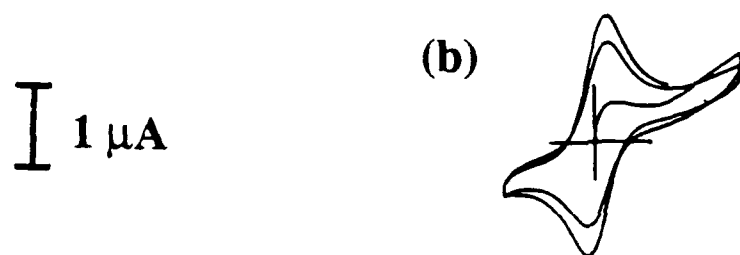
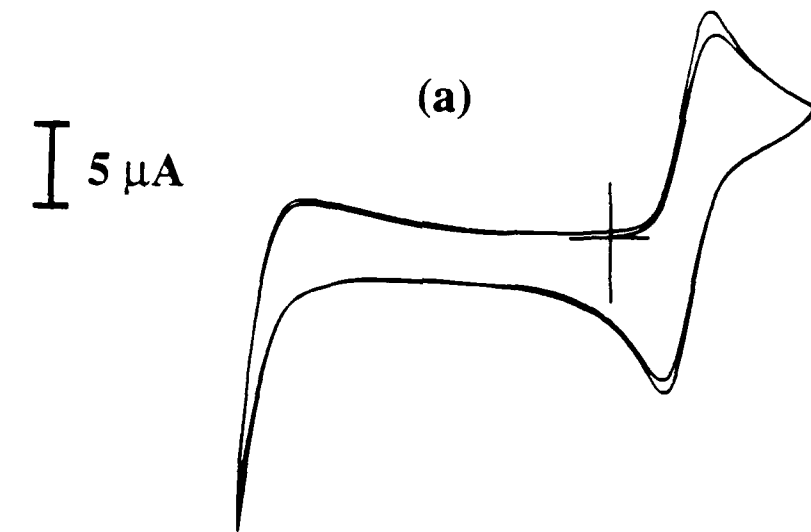


Fig. 6



Voltage (V)

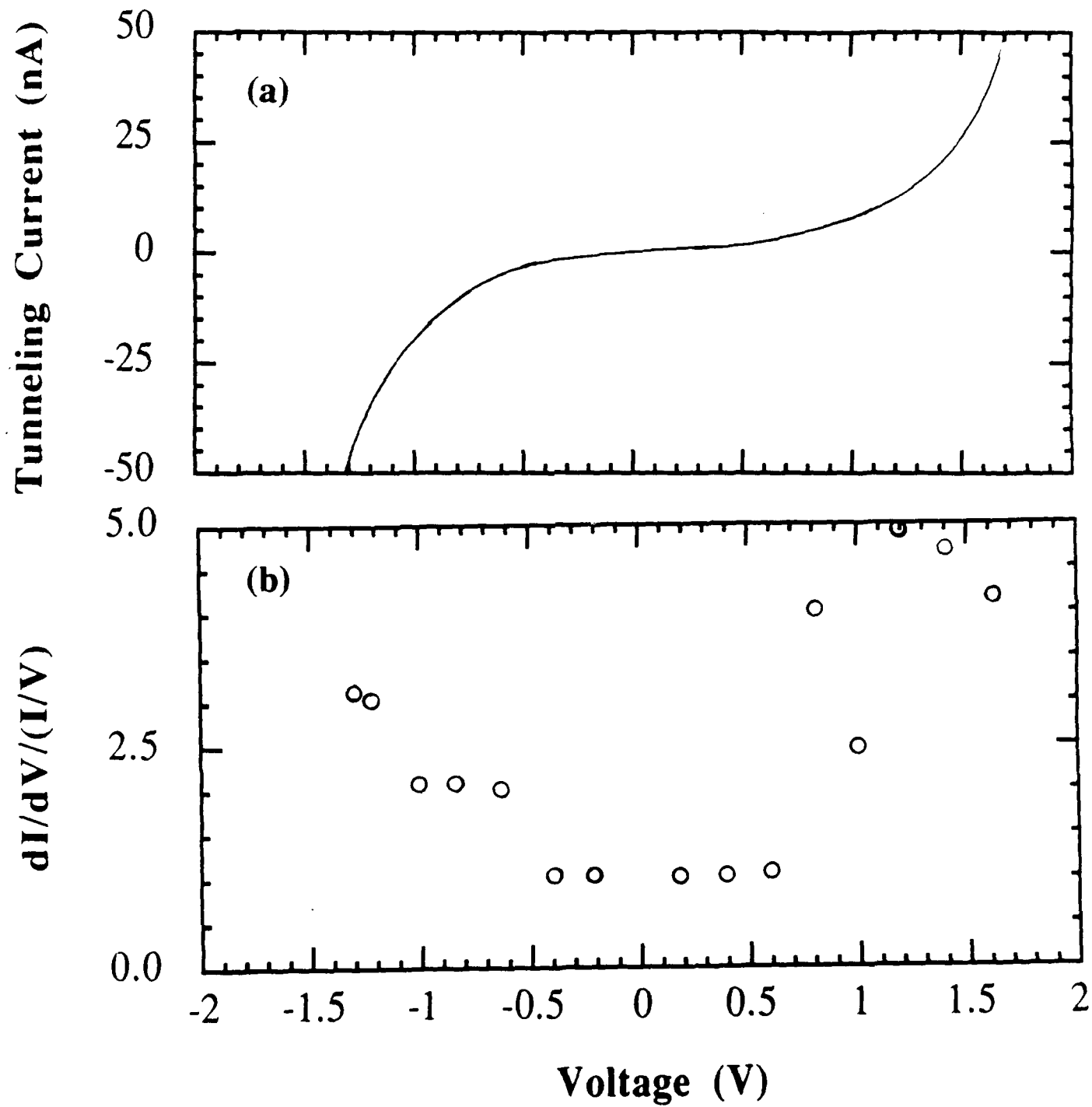


Fig. 8

